OUTLINE FOR GENERALIZED PARTON DISTRIBUTION MEASUREMENTS WITH COMPASS AT CERN

1. Introduction

One of the main open questions in the theory of strong interactions is to understand how the nucleon is built from quarks and gluons, the fundamental degrees of freedom in QCD. An essential tool to investigate nucleon structure is the study of deep inelastic scattering processes where individual quarks and gluons are resolved. The parton densities one can extract from *inclusive* deep inelastic scattering (DIS) describe the distribution of longitudinal momentum ("longitudinal" refers to the direction of the fast moving nucleon in the centre of mass of the virtual photon - nucleon collision). Nevertheless they do not carry any information about the distribution of partons in the transverse plane. In this sense inclusive deep inelastic scattering provides us with a 1-dimensional image of the nucleon. In recent years it has become clear that much more detailed information, encoded in generalized parton distribution (GPDs) [1, 2, 3] can be obtained from hard *exclusive* processes such as deeply virtual Compton scattering (DVCS) and hard exclusive meson production (HEMP). The transverse component of the non-zero momentum transfer between the initial and final nucleon gives access to information about the spatial distribution of partons in the transverse plane. This "mixed" longitudinal parton momentum and transverse coordinate representation provides a 3-dimensional image of the partonic structure of the nucleon [4, 5, 6].

Not only the momentum but also the polarization of the target can be changed by hard exclusive scattering, which leads to a rich spin structure of GPDs. The GPDs will help to unravel the nucleon spin puzzle because they provide, thanks to a sum rule [1], a measurement of the total angular momentum carried by partons, comprising the spin and the orbital angular momentum. Moreover it has also been shown that the GPDs make a connection between ordinary parton distributions and elastic form factors and hence between the principal quantities which so far have provided information on nucleon structure.

At present GPDs are still mostly unknown, apart from constraints from their generic properties linked to parton densities and form factors. Physically we can expect that the dynamics of partons will give rise to separation between fast and slow partons, quarks and gluons, in their transverse spatial distribution. For example lattice calculations [7] have shown that slow partons tend to stand at a larger distance from the nucleon centre than the fast partons. The chiral dynamics approach [8] has also demonstrated that at larger transverse distance the gluon density is generated by the "pion cloud" of the nucleon which implies that the transverse size of the nucleon increases if x_{Bj} drops significantly below m_π/m_N. This is the kinematical domain of study at COMPASS. Knowledge of the transverse size of parton distribution, which is reachable by hard exclusive lepto-production of photons or mesons, is indubitably interesting in itself, and will provide also important parameters in modeling hadron-hadron collisions such as at LHC or RHIC.

We propose to use the 100 GeV muon beam at CERN to study both HEMP and DVCS after 2010 once the present COMPASS program is achieved.

2. Factorization and GPDs

In this section we briefly review the formalism and the properties of the Generalized Parton Distributions (GPDs). We recall that in the DIS regime (corresponding to an incoming virtual photon γ^* of characteristics $Q^2, \nu \to \infty$ and $x_{Bj} = Q^2/2m_N\nu$ finite), the ordinary parton distribution $q(x)$ gives the *probability* for finding a parton q carrying a longitudinal momentum fraction x in the fast moving proton. The optical theorem relates the DIS cross section to the imaginary part of the forward virtual Compton amplitude:

$$\sigma_{DIS} = \sum_X |\gamma^*p \to X|^2 \quad \propto \quad \mathcal{I}m(\gamma^*p \to \gamma^*p)_{t=0} = \sum_q e_q^2 [xq(x)]_{x=x_{Bj}} \tag{1}$$

Deeply Virtual Compton Scattering is a natural extension of the previous case with the difference that the final proton receives a momentum transfer $\Delta = p' - p$, which gives skewedness compared with the inclusive case, as illustrated in Fig. 1. Ji *et al.* [1], Radyuskin [2] and Collins *et al.* [9] have
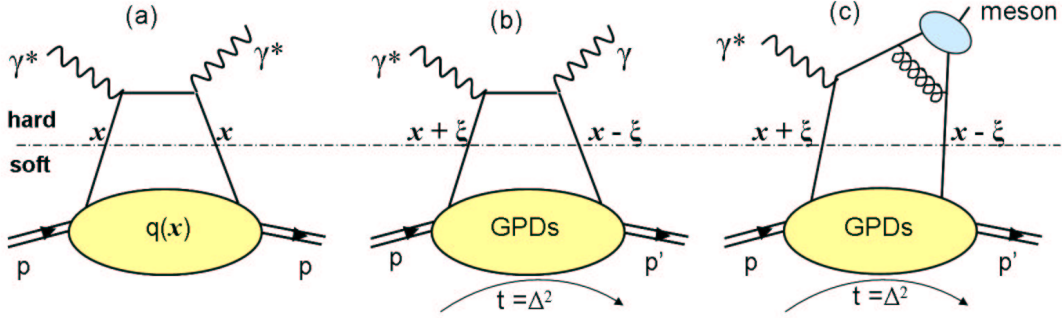

Fig. 1: Handbag diagram for the forward Compton amplitude (a) $\gamma^*p \to \gamma^*p$ whose imaginary part gives the DIS cross section; Handbag diagrams for the DVCS (b) and HEMP (c) amplitudes described at leading order.

shown that the deeply virtual Compton scattering can be factorized into a hard-scattering part (exactly calculable in pQCD) and a non-perturbative nucleon structure part. The factorization is valid when the finite momentum transfer $t = \Delta^2$ to the target remains small comparatively to the photon virtuality Q^2. In the so-called "handbag" diagram, the lower blob represents the soft structure of the nucleon and can be described, at leading order in $1/Q$, in terms of four Generalized Parton Distributions, which conserve quark helicity: they are $H, \tilde{H}, E$ and $\tilde{E}$.

The GPDs reflect the structure of the nucleon independently of the reaction which probes the nucleon. They can also be accessed through the hard exclusive electroproduction of mesons $\pi, \rho^0, \omega,$ $\phi...$ for which the factorization [9] implies the extra condition that the virtual photon be longitudinally polarized.

The GPDs depend upon three kinematical variables: x, ξ and t. x is the average longitudinal momentum fraction of the active quarks in the quark loop (see Fig. 1). ξ is the longitudinal momentum fraction of the transfer Δ necessary to transform a virtual photon into a real photon or a meson, and is related to x_{Bj} as $\xi = x_{Bj}/(2 - x_{Bj})$ in the Bjorken limit. $t = \Delta^2$ is the transfer between the initial and final nucleons, which contains in addition to the longitudinal component a transverse one. This leads to information about the spatial transverse distribution of partons in addition to the longitudinal momentum distribution.

H and $\tilde{H}$ are generalizations of the parton distributions measured in DIS. In the forward limit, corresponding to $\xi = 0$ and $t = 0$, H^q reduces to the quark distribution $q(x)$ and $\tilde{H}^q$ to the quark-helicity distribution $\Delta q(x)$ measured in DIS while for gluons one has $H^g(x,0,0) = g(x)$ and $\tilde{H}^g(x,0,0) = \Delta g(x)$. H and $\tilde{H}$ conserve the helicity of the proton, whereas E and $\tilde{E}$ allow for the possibility that the proton helicity is flipped. In such a case the overall helicity is not conserved: the proton changes helicity

2

but the massless quark does not, so that angular momentum conservation implies a transfer of orbital angular momentum. This is only possible for nonzero transverse momentum transfer, which is new with respect to the ordinary parton distributions. That the GPDs involve the orbital angular momentum of the partons is epitomized in Ji's sum rule [1], which states that the second moment

$$\frac{1}{2} \sum_q \int_{-1}^{+1} dx\, x (H^q(x, \xi, t = 0) + E^q(x, \xi, t = 0)) = J^{quark} \tag{2}$$

at $t = 0$ gives the total (spin + orbital) angular momentum carried by the quarks. It exists an equivalent sum rule for gluons.

In the parton interpretation, the initial parton carries the longitudinal momentum fraction $x + \xi$ (cf Fig. 1), while the longitudinal momentum fraction of the returning parton is $x - \xi$. The GPDs represent the *interference* between the wave functions representing these two different nucleon states. GPDs thus correlate different parton configurations in the hadron at the quantum mechanical level. The kinematical regime $|x| \leq \xi$ where the initial hadron emits a quark-antiquark or gluon pair (or a meson) has no counterpart in the usual parton distributions and carries information about the $q\bar{q}$ and gg components in the hadron wave function.

The first moments of the GPDs are related to the standard hadronic form factors. For any ξ, one has:

$$\sum_q e_q \int_{-1}^{+1} dx\, H^q(x, \xi, t) = F_1(t), \qquad \sum_q e_q \int_{-1}^{+1} dx\, \tilde{H}^q(x, \xi, t) = g_A(t),$$

$$\sum_q e_q \int_{-1}^{+1} dx\, E^q(x, \xi, t) = F_2(t), \qquad \sum_q e_q \int_{-1}^{+1} dx\, \tilde{E}^q(x, \xi, t) = h_A(t) \tag{3}$$

where e_q is the electric charge of the relevant quark. F_1, F_2 are the Dirac and Pauli form factors respectively, g_A is the axial form factor and h_A is the pseudoscalar form factor. A simple physical interpretation of GPDs has thus emerged [4, 5, 6]: they quantify the contribution of quarks with longitudinal momentum fraction x to the corresponding form factor. Given the fact that one can associate the Fourier transform of form factors with charge distributions in position space, it is very tempting to expect that GPDs also contain some information about the distribution of partons in position space. It is clearly established [4] that for $\xi = 0$, $H(x, 0, -\Delta_\perp^2)$ is the Fourier transform of the probability density to find a quark with momentum fraction x at a given distance $b_\perp$ from the center of momentum in the transverse plane: $H(x, 0, -\Delta_\perp^2) = \int d^2 b_\perp e^{-i\Delta_\perp \cdot b_\perp} f(x, b_\perp)$. The width of the $b_\perp$ distribution goes to zero as $x \to 1$ since the active quark becomes the center of momentum. One expects quarks at large x to come from the more localized valence "core" of the nucleon, while the small x region should receive contributions from the much wider meson "cloud" and therefore one would expect a gradual increase of the t-dependence of $H(x, 0, t)$ as one goes from larger to smaller values of x. This is the basis of the 3 dimensional description of the nucleon structure illustrated for example by recent lattice calculations [7] or chiral dynamics approach [8].

3. Goal of GPDs measurements with the high energy muon beam

A complete experiment of both Hard Exclusive Meson Production (HEMP) with a large set of mesons ($\rho, \omega, \phi, \pi, \eta...$) and Deeply Virtual Compton Scattering (DVCS) can be performed with the 100 GeV muon beam and the high resolution COMPASS spectrometer completed by a recoil detector for which outline will be described in the last section.

3.1 Complementarity of the kinematic domains investigated at JLab, DESY and CERN

Experiments have already been undertaken at very high energy at the HERA collider [10, 11] to study mainly the gluon GPDs at very small x_{Bj} ($\leq 10^{-2}$). Larger values of x_{Bj} have been investigated in

3

fixed target experiments at JLab [12] (at 6 GeV, with an upgrade at 11 GeV planned around 2010) and HERMES [13] (at 27 GeV). The goal of an experiment is to study DVCS and HEMP at fixed x_{Bj} in a large range in Q^2 in order to control the factorization and the dominance of the handbag diagram for the studied reaction (see Fig 1). Fig. 2 shows that the maximum energy of the lepton beam will give a limit to the domain in Q^2 at fixed x_{Bj} so the high energy of the muon beam provides a large advantage to COMPASS. The experimental program using COMPASS at CERN with a muon beam of 100 GeV will give access mainly to three bins in x_{Bj} (presented in Fig. 2):

$$x_{Bj} = 0.05 \pm 0.02$$
$$x_{Bj} = 0.1 \pm 0.03$$
$$x_{Bj} = 0.2 \pm 0.07 \tag{4}$$

in a large range of Q^2 ($1.5 \leq Q^2 \leq 7.5$ GeV^2). The range in Q^2 for COMPASS is at present limited up to 7.5 GeV^2 not due to the energy of the muons but due to a reasonable time of 6 months for data taking to realize a DVCS experiment [1], assuming a muon flux of $2 \cdot 10^8$ μ per SPS spill. It has to be noted that an increase of the number of muons per spill by a factor 2 would increase the range in Q^2 up to about 11 GeV^2.
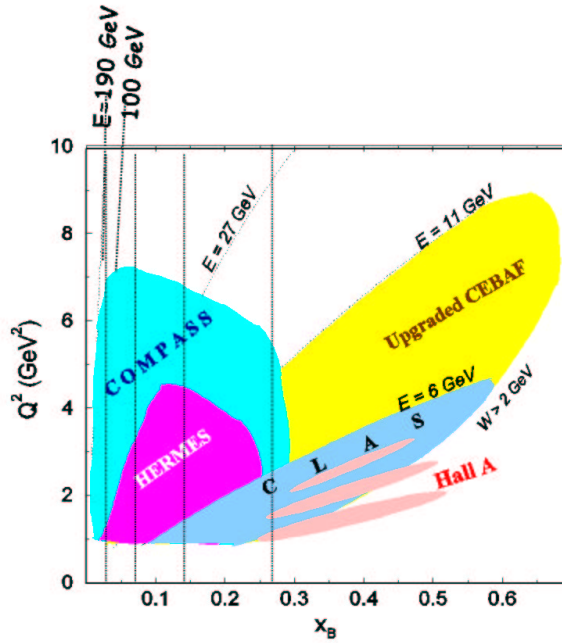

Fig. 2: Kinematical coverage for various planned or proposed experiments. The limit $s \geq 6$ GeV^2 assures to be above the resonance domain, and $Q^2 > 1.5$ GeV^2 allows to reach the Deep Inelastic regime. The range in Q^2 at COMPASS is at present limited up to 7.5 GeV^2 due to the luminosity determined by a maximum of $2 \cdot 10^8$ μ per SPS spill.

At COMPASS one can explore a domain of intermediate x_{Bj} which is sensitive to both valence and sea quarks as well as gluons. As it has been reported in the introduction, the chiral dynamics approach developed by Strikman and Weiss [8] shows that at larger transverse distance from the nucleon centre, the gluon density is generated by the "pion cloud" and so the transverse size of the nucleon increases if x_{Bj} drops significantly below m_π/m_N. This can be studied in the kinematical domain of COMPASS.

3.2 DVCS

Deeply virtual Compton scattering is accessed by photon lepto-production: $lp \rightarrow l'p'\gamma$. In this reaction, the final photon can be emitted either by the leptons (Bethe-Heitler process) or by the proton (genuine

---

[1]It is the case for DVCS and for production of most of the mesons, except for ρ where we can reach higher Q^2.

DVCS process). Which mechanism dominates at given Q^2 and x_{Bj} depends mainly on the lepton beam energy E_l. Large values of $1/y = 2m_pE_lx_{Bj}/Q^2$ favor DVCS and small values of $1/y$ favor Bethe-Heitler. The Bethe-Heitler process is completely calculable in QED, with our knowledge of the elastic form factor at small t. The high energy muon beam available at CERN allows one to play with the kinematics to favor one of these two processes.

When the DVCS contribution dominates over the BH contribution, the cross section is essentially the square of the DVCS amplitude which, at leading order, has the form:

$$\mathcal{A}(\gamma_T^*) \sim \int_{-1}^{+1} \frac{f(x,\xi,t)}{x-\xi+i\epsilon}dx \quad \sim \quad \mathcal{P}\int_{-1}^{+1} \frac{f(x,\xi,t)}{x-\xi}dx - i\pi f(\xi,\xi,t) \tag{5}$$

where $\mathcal{A}$ represents the dominant $\gamma^*p \to \gamma p$ amplitudes for the transverse γ^* polarization and f stands for a generic GPD and $\mathcal{P}$ for Cauchy's principal value integral. The kinematics fixes t and $\xi \sim x_{Bj}/2$.

Since GPDs are real valued due to time reversal invariance, the real and imaginary parts of the DVCS amplitude contain very distinct information on GPDs. The imaginary part depends on the GPDs at the specific values $x = \xi$. The real part is a convolution of the GPDs with the kernel $1/(x-\xi)$ (see Eq. 5). To extract the GPDs from this convolution our strategy will be similar to the one used in DIS. The GPDs will be adequately parametrized and the parameters will be determined by a fit to the data.

The real and imaginary parts can be accessed separately through the interference between BH and DVCS. To see how it works [14, 15, 16], let us consider an unpolarized target and discuss the dependence of the cross section on the angle φ between leptonic and hadronic planes, and on the charge e_l and longitudinal polarization P_l of the muon beam. We schematically have:

$$\frac{d\sigma(\ell p \to \ell p \gamma)}{d\varphi}$$
$$= A_{BH}(\cos\varphi, \cos2\varphi, \cos3\varphi, \cos4\varphi)$$
$$+ A_{INT}(\cos\varphi, \cos2\varphi)[\ e_\ell\ [c_1 \cos\varphi\ \Re e\mathcal{A}(\gamma_T^*)\ +\ c_2 \cos2\varphi\ \Re e\mathcal{A}(\gamma_L^*)\ +\ ...]$$
$$+ e_\ell P_\ell\ [s_1 \sin\varphi\ \Im m\mathcal{A}(\gamma_T^*)\ +\ s_2 \sin2\varphi\ \Im m\mathcal{A}(\gamma_L^*)\ ]]$$
$$+ A_{VCS}(\cos\varphi, \cos2\varphi, P_\ell \sin\varphi) \tag{6}$$

where A_{BH}, A_{VCS}, A_{INT}, c_i, s_i are known expressions and $\mathcal{A}$ represents $\gamma^*p \to \gamma p$ amplitudes for different γ^* polarization. The scaling predictions give leading twist-2 and twist-3 contributions for $\mathcal{A}(\gamma_T^*)$ and $\mathcal{A}(\gamma_L^*)$ respectively. With muon beams one naturally reverses both charge and helicity at once, but we see how all four expressions in the interference can be separated: in the cross section difference $\sigma(\mu^{+\downarrow}) - \sigma(\mu^{-\uparrow})$ the Bethe-Heitler contribution A_{BH} drops out and one has access to the real parts of $\mathcal{A}(\gamma_{T,L}^*)$. Using angular analysis one can separate $\mathcal{A}(\gamma_T^*)$ and $\mathcal{A}(\gamma_L^*)$ which allows a test of the scaling predictions $\mathcal{A}(\gamma_T^*) \sim Q^0$ and $\mathcal{A}(\gamma_L^*) \sim Q^{-1}$ of the factorization theorem. In the sum of the cross section $\sigma(\mu^{+\downarrow}) + \sigma(\mu^{-\uparrow})$ the imaginary parts of $\mathcal{A}(\gamma_{T,L}^*)$ can be separated from the Bethe-Heitler and VCS contributions by their angular dependence, since their coefficients change sign under $\varphi \to -\varphi$ whereas the other contributions do not.

Figure 3 shows the azimuthal distribution of the beam charge asymmetry (BCA) which could be measured at COMPASS with 100 GeV muon beams for different (x_{Bj}, Q^2) domains. Statistical errors are evaluated for 150 days of data taking with a 25% global efficiency. The data allow a good discrimination between different models. Model 1 [17] uses a simple ansatz to parametrize GPDs based on nucleon form factors and parton distributions and fulfills the GPD sum rules. Model 2 [18, 19] is more realistic because it correlates the x and t dependence. This takes into account the fact that the slow partons tend to stand at a larger distance from the nucleon centre than the fast partons. A gradual increase of the t-dependence of $H(x,0,t)$ is considered as one goes from larger to smaller values of x. The parametrization: $H(x,0,t) = q(x)e^{t<b_\perp^2>} = q(x)/x^{\alpha t}$ is used where $<b_\perp^2> = \alpha \cdot ln 1/x$ represents the increase of the nucleon transverse size with energy. The domain of intermediate x_{Bj} reachable at
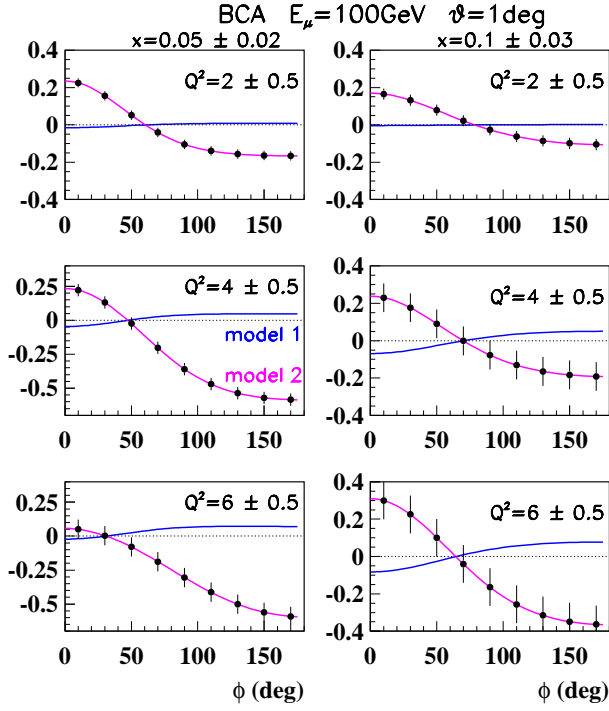
Fig. 3: Projected error bars for a measurement of the azimuthal angular distribution of the beam charge asymmetry measurable at COMPASS at E_μ= 100 GeV and $|t| \leq 0.6$ GeV^2 for 2 domains of x_{Bj} (x_{Bj} = 0.05±0.02 and x_{Bj} = 0.10±0.03) and 3 domains of Q^2 ($Q^2 = 2\pm0.5$ GeV^2, $Q^2 = 4 \pm 0.5$ GeV^2 and $Q^2 = 6 \pm 0.5$ GeV^2) obtained in 150 days of data taking with a global efficiency of 25% and with $2 \cdot 10^8$ μ per SPS spill ($P_{\mu+} = -0.8$ and $P_{\mu-} = +0.8$) and a 2.5m long liquid hydrogen target
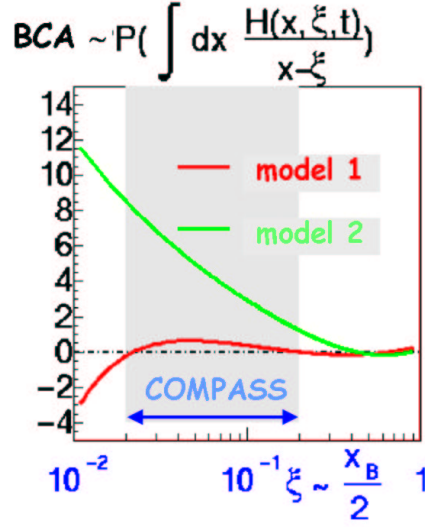

Fig. 4: The beam charge asymmetry (BCA) is mainly controlled by the real part of DVCS amplitude and this figure presents the evolution of this amplitude for the dominant GPD H as a function of x_{Bj}. The domain which can be investigated at COMPASS gives large deviation between the models 1 and 2, where only the last model takes care about the different spatial distributions for fast and slow partons.

COMPASS is related to the observation of sea quarks or meson "cloud" or also gluons and it provides a large sensitivity to this three-dimensional picture of partons inside a hadron as we can see it in Fig. 4 and as it was suggested by the chiral approach [8].

3.3 HEMP

The GPDs reflect the structure of the nucleon independently of the reaction which probes the nucleon. In this sense they are universal quantities and can also be accessed, through DVCS (just previously reviewed) or through the hard exclusive leptoproduction of mesons as $\pi^{0,\pm}, \eta, ..., \rho^{0,\pm}, \omega, \phi, ...$.

Nevertheless these last processes involve a second non-perturbative quantity which is the meson distribution amplitude, describing the coupling of the meson to the $q\bar{q}$ (or gluon) pair produced in the hard scattering (see Fig. 1). This complexity leads to more constraints in the applicability of the GPDs formalism which relies on factorization. According to Collins, Frankfurt and Strikman [9], the factorization applies only when the virtual photon is longitudinally polarized. The authors also demonstrate that the cross section is suppressed by $1/Q^2$ when the virtual photon is transversely polarized.

The different scaling predictions [17] for photon and meson production are shown in Fig. 5. In leading twist the DVCS cross section $d\sigma/dt$ is predicted to behave as $1/Q^4$ whereas the meson longitu-

dinal cross sections will obey a $1/Q^6$ scaling (due to the "extra" gluon exchange for the mesons. It is clear that the production of ρ^0 vector meson provides the largest counting rates comparatively to other mesons. With its decays in 2 charged particles whose invariant mass gives a clear resonance signal, this channel can be easily selected with the present COMPASS spectrometer and is already be investigated.
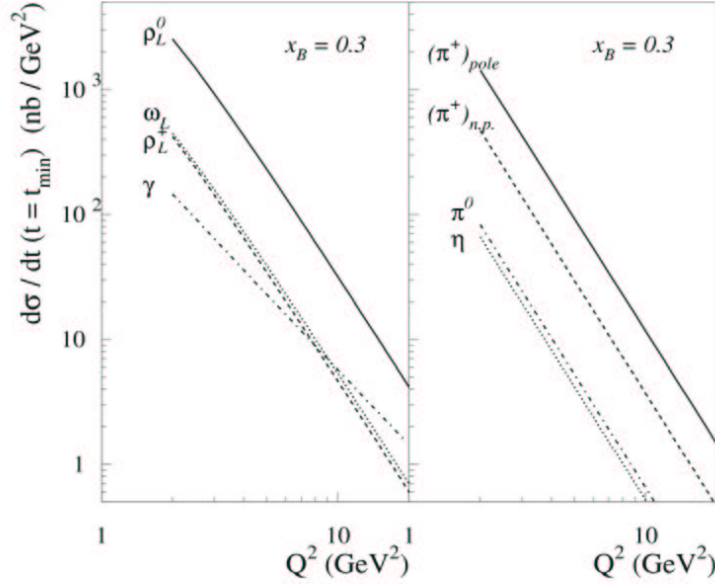

Fig. 5: Scaling behavior of the leading order predictions [17] for the forward differential leptoproduction cross section $d\sigma_L/dt$ on the proton for vector mesons (left panel) and pseudo scalar mesons (right panel). Also shown is the scaling behavior of the forward DVCS cross section (dashed-dotted line in left panel).

In case of production of pseudo-scalar meson (with spin zero) where its polarization is unobserved, one needs to extract the longitudinal cross section from $\sigma_T + \epsilon\,\sigma_L$ by a Rosenbluth separation requiring two different beam energies. For production of ρ meson (or for any vector meson) the angular distribution of decay $\rho \to \pi^+\pi^-$ contains information on the ρ helicity. Experimental data obtained at NMC [20], E665 [21], ZEUS [24], H1 [25] and presently at COMPASS [27, 28] have indicated that the helicity of the photon in the γ^*p centre of mass system is approximatively retained by the vector meson, a phenomenon known as s-channel helicity conservation (SCHC). This can be used to translate a measurement of the cross sections for transverse and longitudinal ρ mesons into a measuremerent of σ_T and σ_L for transverse and longitudinal photons, without resorting to Rosenbluth separation.

The validity of SCHC can be tested in details with the complete angular distribution of the meson production obtained with a longitudinal polarized beam (such as at COMPASS) which provides the full set of ρ density matrix elements. The analyses of the present COMPASS data [27, 28] demonstrate a copious production of ρ^0 mesons, in a range of Q^2 significantly larger than those of the previous experiments. Fig. 6 presents the ratio $R = \sigma_L/\sigma_T$ determined by the decay angular distribution. The 2002 COMPASS data are limited to Q^2 up to about 5 GeV^2 while the new 2003 data due to the enlarged Q^2 trigger will provide results up to 27 GeV^2. The ratio R increases with Q^2 and reaches a value larger than 1 at Q^2 around 2 or 3 GeV^2, providing a favorable case for GPDs study that the longitudinal contributions become dominant. This is agreement with Collins' predictions [9].

The longitudinally polarized vector meson channels $\rho^{0,\pm}, \omega, \phi, ...$ are sensitive only to the GPDs H and E while the pseudo-scalar channels $\pi^{0,\pm}, \eta, ...$ are sensitive only to $\tilde{H}$ and $\tilde{E}$ [9] . In comparison we recall that DVCS depends on the four GPDs: H, E, $\tilde{H}$ and $\tilde{E}$. This property makes the hard meson production reactions complementary to the DVCS process as it provides an additional tool or filter to disentangle the different GPDs.
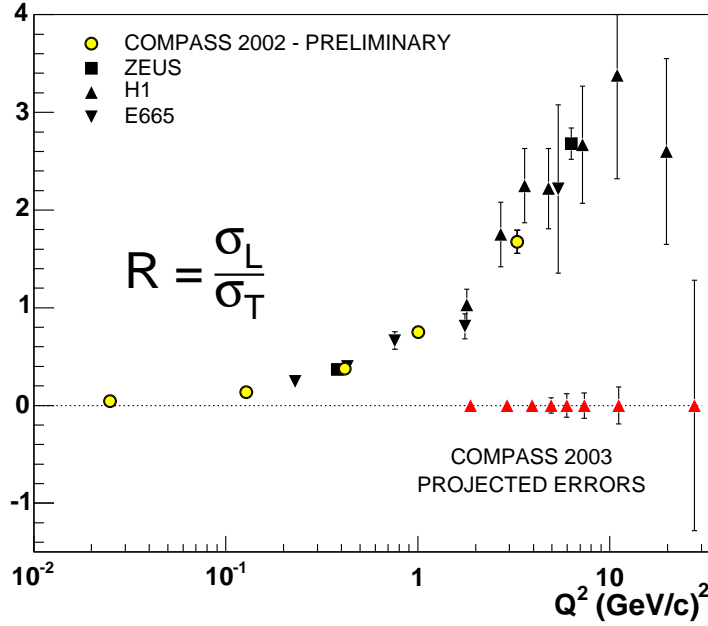
Fig. 6: $R = \sigma_L/\sigma_T$ obtained with the spin density matrix element r_{00}^{04} determined from the ρ decay angular distribution. The COMPASS 2002 preliminary results are compared to the published data of E665 [21], ZEUS [24], H1 [25]. Also are shown the estimated errors for COMPASS 2003 due to the enlarged Q^2 trigger.

Quark and gluon GPDs contribute both for the meson production as the GPDs for gluons enter at the same order in α_s as those for quarks. Decomposition on flavor quark and gluon contributions can be realized through the different combinations obtained with a set of mesons. For example:

$$
\begin{aligned}
H_{\rho^0} &= \frac{1}{\sqrt{2}}\left(\frac{2}{3}H^u + \frac{1}{3}H^d + \frac{3}{8}H^g\right) \\
H_\omega &= \frac{1}{\sqrt{2}}\left(\frac{2}{3}H^u - \frac{1}{3}H^d + \frac{1}{8}H^g\right) \\
H_\phi &= -\frac{1}{3}H^s - \frac{1}{8}H^g
\end{aligned}
\tag{7}
$$

The relative production of these three meson ρ:ω:ϕ will give ratios as 9:1:2 in the region where the gluon GPDs dominate over those for quarks. How important are the respective contributions at intermediate x_{Bj} and from which point quarks start to dominate is not clear at present. Studies by Vanderhaeghen, Guichon and Guidal [17] have added the cross sections modeled for quarks GPDs [17] (model 1 of the previous section) and gluon GPDs [26] but not taken into account their interference (see Fig. 7). These predictions show that at small x_{Bj} (domain of ZEUS [22, 23]) the gluon contribution dominates while at intermediate x_{Bj} (domain of NMC [20] and E665 [21]) the valence quark contribution is also important. The expected errors for the COMPASS 2003 data, which are also shown in Fig. 7, are encouraging for this study.

Besides the cross section σ_L, there is one more observable which can be expressed using the factorization theorem. It is the single spin asymmetry for a transversely polarized target again with a longitudinal photon. This experiment can be realized right now with the COMPASS setup and the polarized target during the transversity measurements. This asymmetry is directly proportional to the ratio E/H. Note that the contribution of GPD E is always screened by to the dominant contribution of the GPD H either in the DVCS cross section or single spin asymmetry or beam charged asymmetry or in the longitudinal cross section for vector mesons. So the transverse spin asymmetry provides a favorable case to measure the GPD E. This is essential to study Ji's sum rule and nucleon spin puzzle. Sensitivity
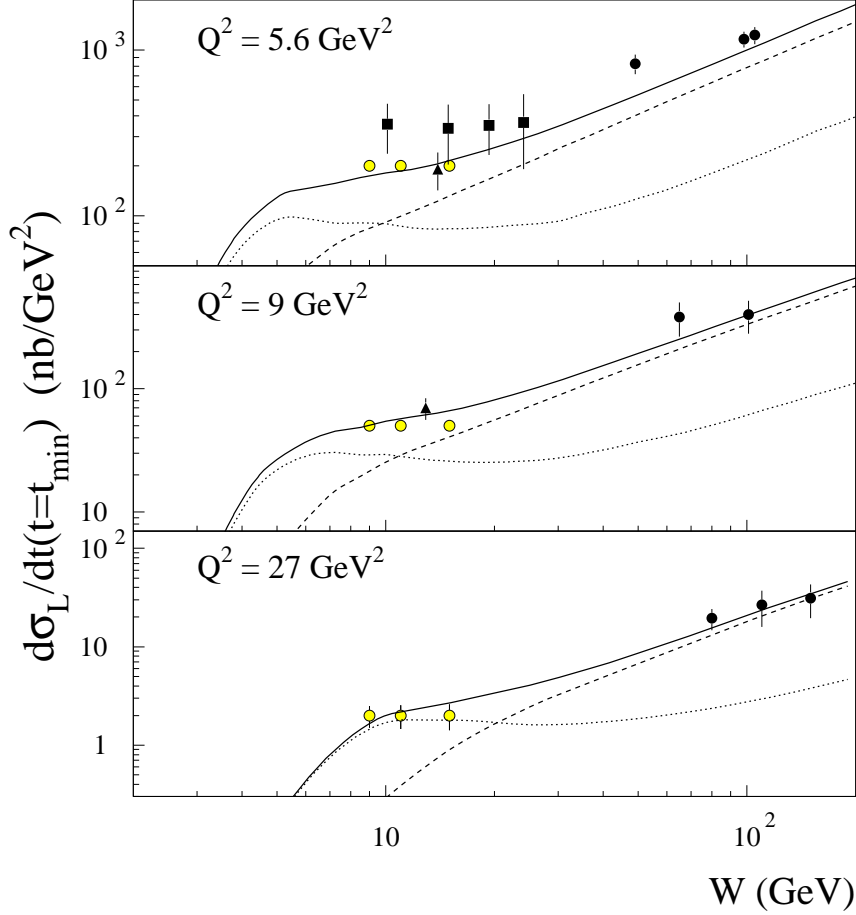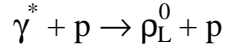
8

$$\gamma^* + p \rightarrow \rho_L^0 + p$$

Fig. 7: Longitudinal forward differential cross section for ρ_L^0 production (Fig. from [17]). Predictions reproduce quark contributions (dotted lines), gluon contributions (dashed lines) and the sum of both (full lines). The data are from NMC (triangles) [20], E665 (squares) [21], ZEUS 93 [22] and ZEUS 95 [23] (solid circles). Also are shown the expected errors for the COMPASS 2003 data (with the open circles at W=9, 11, 14 GeV).

to the parametrization of the GPD E which is very poorly known, is reported in the reference [18] and seems encouraging in the intermediate x_{Bj} domain of COMPASS.

Precise simulations of exclusive ρ^0 and π^0 production have already been performed [29, 30] and it is undoubtedly that hard exclusive meson production (HEMP) and DVCS, which can be realized at the same time in the same setup, provide different and complementary facets for the GPDs study.

4. Beam and target requirements

4.1 Highest luminosity requirement

The highest luminosity reachable at COMPASS is required to investigate these exclusive measurements. These experiments will use 100-190 GeV/c muons from the M2 beam line. Presently limits on radioprotection in the experimental hall imply that the maximum flux of muons be expected is of $2 \cdot 10^8$ muons per SPS spill (5.2s spill duration, repetition each 16.8s). Under these circumstances, we can reach a luminosity of $\mathcal{L} = 4 \cdot 10^{32}$ cm^{-2}s^{-1} with the present polarized ^{6}LiD or NH$_3$ target of 1.2 meter

length, and only $\mathcal{L} = 1.3 \cdot 10^{32}$ cm^{-2}s^{-1} with a new liquid hydrogen target of 2.5 meter length which has to be designed for this proposal.

It is important to note that these experiments will benefit directly from every improvement of the muon flux in order to increase statistics and enlarge the kinematical domain in Q^2.

4.2 Absolute luminosity determination (as in NMC)

In order to get useful cross sections, it is necessary to perform a precise absolute luminosity measurement. This has already been achieved by the NMC Collaboration within a 1% accuracy [31]. The integrated muon flux was measured continuously by two methods: either by sampling the beam with a random trigger (provided by the α emitter Am^{241}) or by sampling the counts recorded in 2 scintillators hodoscope planes used to determine incident beam tracks. The beam tracks were recorded off-line, in the same way as the scattered muon tracks to determine exactly the integrated usable muon flux.

4.3 Positive and negative muon beam of opposite polarization and same intensity

μ^+ and μ^- beams of 100 GeV energy, with the largest intensity as well as exactly opposite polarization (to a few %) are required. The muons are provided by pion and kaon decay and are naturally polarized. The pions and kaons come from the collision of the 400 GeV proton beam (of $1.2 \cdot 10^{13}$ protons per SPS cycle) on a Be primary target. A solution [32] is under study and consists in:
1) selecting 110 GeV pion beams from the collision and 100 GeV muon beams after the decay section in order to maximize the muon flux;
2) keeping constant the collimator settings which define the pion and muon momentum spreads (both the collimator settings in the hadron decay section and the scrapper settings in the muon cleaning section) in order to fix the μ^+ and μ^- polarizations at exactly the opposite value ($P_{\mu^+} = -0.8$ and $P_{\mu^-} = +0.8$);
3) fixing N_{μ^-} close to $2 \cdot 10^8$ μ per SPS spill with the longest 500mm Be primary target;
4) the number of N_{μ^+} will be about a factor 2 larger than that of N_{μ^-}.

5. Detectors necessary to complement the high resolution COMPASS forward spectrometer

5.1 Necessity to complement the present setup

The outgoing muon scattered in the very forward direction (below $1°$) will be measured in the present high resolution COMPASS spectrometer [33]. The outgoing meson or photon are emitted at larger angle, but below $10°$ in order to intercept the RICH detector or the two COMPASS calorimeters (ECAL1 + ECAL2) [34, 35], mainly constituted of lead-glass blocks of excellent energy and position resolution and high rate capability. The recoil proton scatters at large angle and small momentum (≤ 750 MeV/c) which cannot be detected by the present COMPASS apparatus. Furthermore the missing mass energy technique using the energy balance of the scattered muon and photon or meson is not accurate enough at such high beam energy (the resolution in missing mass which is required is $(m_p + m_\pi)^2 - m_p^2 = 0.25$ GeV^2 and the experimental resolution which can be achieved is larger than 1 GeV^2). Thus, a recoil detector has to be designed to measure precisely the proton momentum and insure the exclusivity of these exclusive processes.

The DVCS reaction is surely the most delicate reaction to perform because one has to select a final state with one muon, one photon and one low energy proton among many competing reactions listed below:
1) Hard Exclusive π^0 Production $\mu p \rightarrow \mu p \pi^0$ where π^0 decays in two photons, for which the photon with higher energy imitates a DVCS photon, and the photon with smaller energy is emitted at large angle outside of the acceptance or its energy is below the photon detection threshold.
2) Diffractive dissociation of the proton $\mu p \rightarrow \mu \gamma N^*$ with the subsequent decay of the excited state N^* in $N + k\pi$. (The low energy pions are emitted rather isotropically).

3) Inclusive Deep Inelastic Scattering with, in addition to the reconstructed photon, other particles produced outside the acceptance or for which tracks are not reconstructed due to inefficiency.

Moreover one has to take into account a background which includes beam halo tracks with hadronic contamination, beam pile-up, particles from the secondary interactions and external Bremsstrahlung.

5.2 Simulation with PYTHIA in order to optimize the ratio of DVCS events comparatively to DIS events and to determine the best coverage of the detectors

A simulation has been realized in order to define the proper geometry of the detector complementing the present COMPASS setup. The goal was to maximize the ratio of DVCS events over DIS events for a sample of events with one muon and one photon in the COMPASS spectrometer acceptance plus only one proton of momentum smaller than 750 MeV/c and angle larger than $40°$ (typical DVCS kinematics). Using the event generator code PYTHIA 6.1 [36] which generates all Deep Inelastic Scattering (DIS) processes with many γ and π^0 production possibilities, the experimental parameters such as maximum angle and energy threshold for photon detection and maximum angle for charged particle detection have been tuned. With photon detection extended up to 24 degrees and above an energy threshold of 50 MeV and with charged particle detection up to 40 degrees, one observes that the number of DVCS events as estimated with models is more than an order of magnitude larger than the number of DIS events over the whole useful Q^2 range (see Fig. 8).
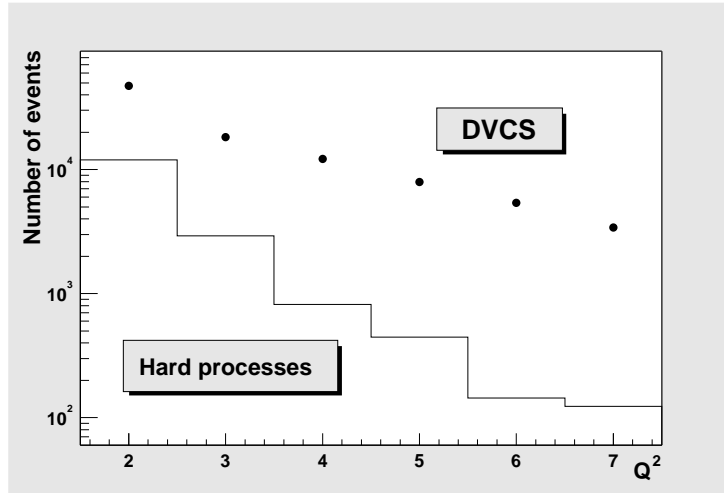

Fig. 8: Number of events for DVCS (dots) and DIS (histogram) processes as a function of Q^2 for selection of events with only one muon, one photon and one recoiling proton and condition for charged particle detection up to 40 degrees and for photon detection up to an angle of 24 degrees and above a threshold of 50 MeV.

5.3 Quality of the calorimetry and extension

The two calorimeters ECAL1 and ECAL2 are necessary for DVCS and π^0 production. They are mainly constituted of lead-glass blocks called GAMS. They are cells of $38.4 \times 38.4 \times 450$ mm^3. Typical characteristics of such calorimeter are:

- energy resolution: $\sigma P_\gamma / P_\gamma = 0.055/\sqrt{P_\gamma} + 0.015$
- position resolution: $\sigma_x = 6.0/\sqrt{P_\gamma} + 0.5$ in mm
- high rate capability: 90% of signal within 50ns gate with no dead time
- effective light yield: about 1 photoelectron per MeV; hence low energy photons of down 20 MeV can be reconstructed.

The separation of the overlapping electromagnetic showers in the cellular GAMS calorimeter is carefully

studied in the Ref. [35]. The result of the study shows that at 10 GeV one can reach a 100% level of the separation efficiency for a minimum distance between 2 photon tracks at the entrance of the calorimeter of D = 4 cm. This excellent performance of the calorimeters will provide a key role in the perfect separation between DVCS events and Hard π^0 events.

Moreover it has been shown with the simulation that it is better to extend the calorimetry from $10°$ up to an angle of $24°$ in order to separate contributions with only one photon, two photons and more.

5.4   Recoil detection

One possible solution to complement the present COMPASS setup is presented in Fig. 9. It consists of one recoil detector described below, an extended calorimetry from 10 to 24 degrees, and a veto for charged forward particles until 40 degrees. This calorimeter has to work in a crowded environment and in a magnetic fringe field of SM1 and therefore it has to be studied further.
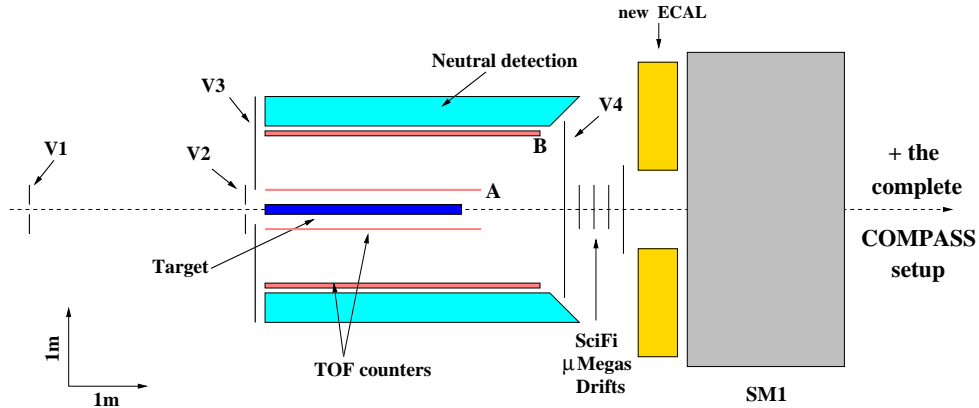

Fig. 9: Proposition for a detector complementing the COMPASS setup. A recoil detector, an extended calorimetry from 10 to 24 degrees, and a veto (V4) for charged forward particles until 40 degrees have been added.

The recoil detector is based on a time of flight (ToF) measurement between two barrels of scintillating slats read at both ends. The inner barrel (noted A) (2.8m length) surrounding the target should be made of slats as thin as possible (4mm) to allow low momentum proton detection. Thicker (5cm) and longer (4m) slats should be used for the outer barrel (noted B). An accurate t measurement implies to achieve a timing resolution of 200ps. External layers of scintillator and lead interleaved should be added to detect extra neutral particles and give an estimate of background. The combination of time of flight measurement and the energy loss in the various sensitive detectors would provide discrimination of events in this fully hermetic detector. We have tested the concept of this detector using the present muon beam at nominal flux and a simplified setup (one sector of reduced length). Resolution of 300ps has been achieved. The performance of this ToF system is limited by the number of photo-electrons that are collected, dispersion due to counter length and high rates. Extension to long (about 4m) scintillators has to be studied carefully and technology has to be improved to achieve still better resolution. The construction of a fully functional prototype segment of the appropriate length is part of the European Initiative I3HP devoted to GPDs study in the FP6 framework (2004-2006).

References

[1] X. Ji, Phys. Rev. Lett. **78** (1997) 610, Phys. Rev. **D 55** (1997) 7114.

[2] A.V. Radyushkin, Phys. Rev. **D 56** (1997) 5524.

[3] M. Diehl, Generalized Parton Distributions, DESY-thesis-2003-018, hep-ph/0307382 and references therein.

[4] M. Burkardt, Phys. Rev. **D62** (2000) 071503.

[5] A.V. Belitsky and D. Müller, Nucl. Phys. **A711** (2002) 118.

[6] J.P. Ralston and B. Pire, Phys. Rev. **D66** (2002) 111501.

[7] J.W. Negele *et al*, Nucl. Phys. Proc. Suppl. 128 (2004) 170.

[8] M. Strikman and C. Weiss, Phys. Rev. **D69** (2004) 054012.

[9] J.C. Collins, L. Frankfurt and M. Strikman, Phys. Rev. **D56**, 2982 (1997).

[10] H1 Collaboration, C. Adloff *et al.*, Phys. Lett. **B 517** (2001) 47.

[11] ZEUS Collaboration, S. Chekanov *et al.*, DESY-03-059, Phys. Lett. **B 573** (2003) 46.

[12] CLAS Collaboration, S. Stepanyan *et al.*, Phys. Rev. Lett. **87** (2001) 182002.

[13] HERMES Collaboration, A. Airapetian *et al.*, Phys. Rev. Lett. **87** (2001) 182001.

[14] M. Diehl, T. Gousset, B. Pire, J. Ralston, Phys. Lett. **B 411** (1997) 193.

[15] M. Diehl, contribution to the workshop "Future Physics @ COMPASS", 26-27 September 2002/

[16] A.V. Belitsky, D. Müller, A. Kirchner, Nucl. Phys. **B 629** (2002) 323.

[17] M. Vanderhaeghen, P.A.M. Guichon, M. Guidal, Phys. Rev. **D 60** (1999) 094017.

[18] K. Goeke, M.V. Polyakov, M. Vanderhaeghen, Prog. Part. in Nucl. Phys. 47 (2001) 401.

[19] Model of Reference [18]; implementation by L. Mossé and M. Vanderhaeghen.

[20] NMC Collaboration, M. Arneodo *et al.*, Nucl. Phys. **B 429** (1994) 503.

[21] E665 Collaboration, M.R. Adams *et al.*, Z. Phys. **C 74** (1997) 237.

[22] ZEUS Collaboration, M. Derrick *et al.*, Phys. Lett. **B 356** (1995) 601.

[23] ZEUS Collaboration, J. Breitweg *et al.*, Eur. Phys. J. **C 6** (1999) 603.

[24] ZEUS Collaboration, J. Breitweg *et al*, Eur. Phys. J. **C 12** (2000) 393.

[25] H1 Collaboration, C. Adloff *et al*, Eur. Phys. J. **C 13** (2000) 360;
H1 Collab., C. Adloff *et al*, Phys. Lett. **B 539** (2002) 25.

[26] L.L. Frankfurt, W.Koepf, M. Strikman, Phys. Rev. **D 54** (1996) 3194.

[27] O.A. Grajek, A. Korzenev, A. Sandacz, COMPASS Note 2002-15 (2002).

[28] E. Burtin, N. d'Hose, O.A. Grajek, A. Sandacz, COMPASS Note 2004-12 (2004).

[29] J. Pochodzalla, L. Mankiewicz, M. Moinester, G. Piller, A. Sandacz, M. Vanderhaeghen, hep-ex/9909534.

[30] A. Sandacz, COMPASS Note 2000-1 (2000).

[31] NMC Collaboration, P. Amaudruz *et al.*, Phys. Lett. **B295** (1992) 159; R.P. Mount, Nucl. Instrum. Methods **187** (1981) 401.

[32] L. Gatignon, private communication.

[33] A Proposal for a Common Muon and Proton apparatus for Structure and Spectroscopy, CERN/SPSLC 96-14 and wwwcompass.cern.ch.

[34] V. Poliakov, Presentation of ECAL1 and ECAL2, January 25, 2001.

[35] A.A. Lednev, Separation of the overlapping electromagnetic showers in the cellular GAMs-type calorimeters, Preprint IHEP 93-153 (1993), Protvino, Russia.

[36] PYTHIA 6.1, User's manual, T. Sjöstrand *et al.*, High Energy Physics Event Generation with PYTHIA 6.1, Comput. Phys. Commun. 135 (2001) 238; hep-ph/0010017.